

PoseMaster: Generating 3D Characters in Arbitrary Poses from a Single Image

Hongyu Yan^{1,2*} Kunming Luo^{1*} Weiyu Li¹
 Yixun Liang¹ Shengming Li³ Jingwei Huang² Chunchao Guo² Ping Tan^{1†}
¹Hong Kong University of Science and Technology ²Tencent Hunyuan ³Tencent IEG



Figure 1. Given a single image and arbitrary poses represented by a body skeleton, PoseMaster can generate high-quality 3D characters that maintain the identity of the image while adhering to the pose defined by the skeleton, enabling controllable character generation in arbitrary poses.

Abstract

3D characters play a crucial role in our daily entertainment. To improve the efficiency of 3D character modeling, recent image-based methods use two separate models to achieve pose standardization and 3D reconstruction of the A-pose character. However, these methods are prone to generating distorted and degraded images in the pose standardization stage due to self-occlusion and viewpoints, which further affects the geometric quality of the subsequent reconstruction process. To tackle these problems, we propose PoseMaster, an end-to-end controllable 3D character generation framework. Specifically, we unify pose transformation and 3D character generation into a flow-based 3D native generation framework. To achieve accurate arbitrary-pose control, we propose to leverage the 3D body bones existing in the skeleton of an animatable character as the pose condition. Furthermore, considering the specificity of multi-condition control, we randomly empty the pose condi-

tion and the image condition during training to improve the effectiveness and generalizability of pose control. Finally, we create a high-quality pose-control dataset derived from realistic character animation data to make the model learning the implicit relationships between skeleton and skinning weights. Extensive experiments show that PoseMaster outperforms current state-of-the-art techniques in both qualitative and quantitative evaluations for A-pose character generation while demonstrating its powerful ability to achieve precise control for arbitrary poses.

1. Introduction

The rapid evolution of the digital content industry has made high-quality 3D content creation essential across various domains, including film, video gaming, online streaming, and virtual reality (VR). Traditionally, character modeling has been a labor-intensive process that demands significant time and expertise from skilled artists. This reliance on manual design poses considerable challenges for scalability and efficiency. To address these issues, researchers are in-

*Equal contribution.

†Corresponding authors.

creasingly employing generative models for automated 3D character generation, aiming to simplify the modeling process and reduce production time.

Unlike regular objects, 3D character generation is often closely linked to specific poses, such as A-pose or T-pose, which are crucial for rigging and skinning in animation. This requirement for pose control introduces challenges in 3D character generation. Previous text-based generation methods [8, 22] utilized parameterized models like SMPL [35] to provide templates and achieve pose control. However, the SMPL model is limited in its ability to adjust features such as hair and clothing during pose transformations, resulting in low-quality controllable character generation. In contrast, recent methods like CharacterGen [42] and StdGen [16] aim to generate 3D characters directly from arbitrary-pose images. These approaches employ diffusion models to transform the pose of the input image into canonical multi-view images (e.g., T-pose or A-pose) and then use a Large Reconstruction Model (LRM) [19] to derive the 3D character from these multi-view A-pose images. While these methods improve the quality of generated geometry and enable detailed modeling, they encounter challenges with self-occlusion in 2D images, leading to distortion and degradation during the pose transformation process. Moreover, the separation of pose transformation and 3D reconstruction heightens the dependency on the accuracy of 2D pose transformations, as any distortions and artifacts can significantly compromise the quality of the reconstructed A-pose 3D character. Furthermore, the multi-stage generation pipeline suffers from inefficiencies in training and inference, as well as cumulative errors. Finally, these methods are limited to fixed A-pose character generation and lack the capability for more flexible controls, such as arbitrary-pose generation.

To address these challenges, we propose PoseMaster, an end-to-end controllable 3D character generation framework. By unifying pose transformation and character generation into a single generative framework, we eliminate reliance on 2D pose transformations and mitigate cumulative errors associated with multi-stage generation pipelines. To enable arbitrary-pose control, we introduce a 3D skeleton representation as the pose condition. Specifically, we adopt the framework of recent native 3D generation methods [29, 67] and design a flow-based generative model [33] that utilizes both image and pose as combined conditions to guide the final generation results. To enhance the accuracy of pose control, we leverage the body bones in the 3D skeleton as signals for pose information, providing precise pose data along with sparse 3D structural information. Additionally, to improve the generative model’s generalization capabilities for pose control, we simultaneously input both conditions into the diffusion transformer and randomly mask them with independent probabilities during training.

To ensure the generated 3D character appears natural and physically plausible, we employ a data-driven approach that enables the network to learn the relationship between the skeleton and skinning weights. Consequently, we construct a high-quality AinimePose dataset derived from realistic character animation data. Our experiments demonstrate that PoseMaster outperforms existing A-pose 3D character generation methods, effectively achieving arbitrary-pose 3D character generation within a unified framework. Moreover, the end-to-end approach results in faster generation speeds compared to existing baselines.

In summary, our paper makes the following key contributions:

- An end-to-end controllable generation framework that combines pose transformation and character generation in a unified generation model, achieving efficient controllability while ensuring high-quality geometry.
- A well-designed 3D pose representation, along with a simple yet effective method for condition injection and training, ensures the precision of pose control and enhances the quality and generalization of the generated geometry.
- A curated dataset from realistic character animation data, which enables the model to learn the implicit relationships between skeleton and skinning weights, thereby producing natural and appropriate poses.

2. Related work

2.1. 3D Generation

In recent years, 3D generation has been achieved significant success, which can be split into three categories: SDS-based, LRM-based, and native generation. The earliest generation methods [28, 32, 43, 47] typically leverage the prior knowledge of 2D diffusion models to optimize a randomly initialized radiance field, such as NeRF [36, 55], Gaussian [23, 30, 49, 62], and DMTet [11, 46], through a process known as Score Distillation Sampling (SDS). However, these SDS-based methods usually require a long time to generate a 3D asset. To speed up the generation process, Large Reconstruction Model (LRM) [19] constructs a one-step feed-forward framework to achieve 3D generation. These LRM-based methods [27, 56, 65] usually utilize a series of Transformer [53] blocks to predict the parameters of 3D representations directly. With training on the high-quality data rendered from the Objaverse [14] dataset, LRM-based methods showcase higher efficiency and geometric quality compared with SDS-based works. However, they still face the challenge to generate high-quality mesh, even if some methods [50, 59, 60] add the input views and geometry constraints (e.g., normal and depth). Unlike approaches that rely on 2D supervision, native generation methods adopt 3D representations such as point

clouds [26, 61, 71], meshes [34, 37, 48], and implicit functions [13, 39, 44] to optimize their network. Benefits from direct 3D data optimization, these native generation methods present impressive geometry quality. Most recently, with the emergence of the representation of VecSet proposed by 3DShapeVecSet [63], Clay [67], CraftsMan [29] proposed to build large 3D latent diffusion models to facilitate the effectiveness and generalization of 3D generation. In this paper, we follow these large native generation methods to build a unified framework for arbitrary-pose 3D character generation.

2.2. 3D Character Generation

Different from the general generation methods introduced above, 3D character generation is a specific and challenging task due to data scarcity and additional requirements for pose modeling. Early methods were mainly based on human prior models SMPL [35] and SMPL-X [40], utilizing generative models such as GAN [17] or CLIP models [18] to achieve high-quality human avatar generation. In recent years, to leverage powerful 2D stable diffusion priors, Dreamavatar [8] and AvatarCraft [22] proposed methods utilizing SDS to optimize implicit models initialized human geometry priors from the SMPL model. Following that, DreamHuman [24] proposed adopting ImGHUM [7] as a body prior. DreamWaltz [20], AvatarVerse [64], and AvatarStudio [68] proposed utilizing DensePose-guided ControlNet [66] to improve pose control. TeCH [21] proposed using the DreamBooth model [45] as an SDS guidance model to achieve image-to-avatar generation. TADA [31] proposed distilling 2D diffusion models to optimize the normals and displacements of the SMPL body mesh. These text-driven methods suffer from low-quality geometry and fine-grained control. Recently, to achieve an image-driven pipeline for controllable character generation, CharacterGen [42] first uses a multi-view diffusion model to convert input arbitrary-pose images into A-pose multi-view images, and then reconstructs an A-pose 3D character through a multi-view-based LRM [19]. Building upon CharacterGen, the latest method StdGen [16] introduces a semantic-aware LRM to generate decomposable characters. Although these methods have achieved significant improvements, the multi-stage generation process can lead to cumulative errors. Moreover, performing pose transformations in 2D space is prone to distortion and artifacts, which can adversely affect the geometry quality. In this paper, by integrating the input images and expected poses into a unified 3D native generation framework, we achieve end-to-end 3D character controllable generation, which enhances controllability and generation quality.

3. Preliminary Study

Flow-based generative models aim to transform a simple noise distribution $x_0 \sim \mathcal{N}(0, I)$ into a complex data distribution $x_1 \sim D$ through a sequence of invertible mappings defined by ordinary differential equations (ODEs). Formally, given a time-dependent vector field $v(x_t, t)$ the evolution of a sample follows:

$$\frac{dx_t}{dt} = v(x_t, t), \quad t \in [0, 1], \quad (1)$$

Rectified flow models [33] define the forward process, $x_t = (1-t)x_1 + tx_0$, as straight paths between the data distribution and a standard normal distribution. In this design, the velocity v can be approximated with a neural network v_θ by minimizing the conditional flow matching objective:

$$\mathbb{E}_{t, x_0, x_1} \|v_\theta(x, t) - (x_1 - x_0)\|_2^2. \quad (2)$$

Following this, we can obtain our conditional flow matching objective:

$$\mathbb{E}_{t, x_0, x_1, c_i, c_p} \|v_\theta(x, t, c_i, c_p) - (x_1 - x_0)\|_2^2. \quad (3)$$

where c_i is image condition while c_p is pose condition.

4. Method

In this section, we begin by introducing our data construction to show how we organize our data to achieve arbitrary-pose control generation in Section 4.1. Then, we present how we design our 3D-VAE and Flow-based diffusion network to accomplish high-quality pose control in Section 4.2.

4.1. Dataset Construction

In this work, we aim to achieve arbitrary-pose 3D character generation from an input image and a pose cue. To accomplish this, we require data pairs that consist of an image, a skeleton, and a mesh that accurately represents the appearance and shape corresponding to the image, with the pose defined by the skeleton. However, a large-scale dataset for generating 3D characters with arbitrary poses does not currently exist. To address this gap, we construct our AnimePose dataset, following these main stages:

4.1.1. Data Collecting

We leverage 3D animation data to obtain the required datasets by rendering different frames from motion sequences. By rendering a large number of action frames for a given character, we can construct data pairs by selecting an image from one frame and the corresponding skeleton and ground truth mesh from another frame. Thanks to the MikuMikuDance (MMD) community [3], which provides a wealth of animatable characters with detailed geometry, realistic appearances, and high-quality motion sequences, we

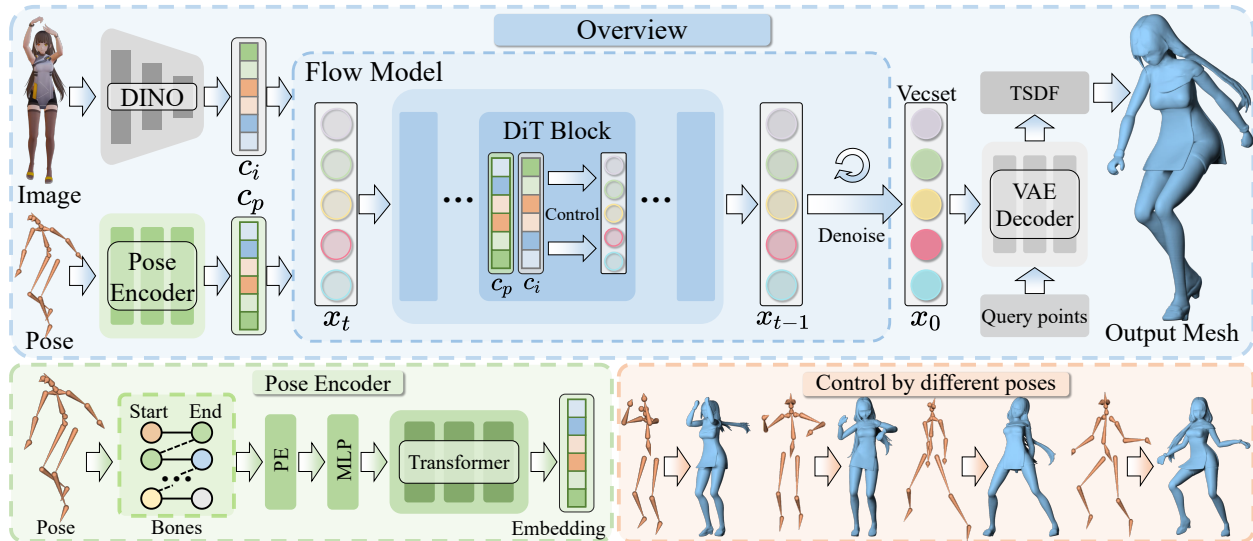


Figure 2. Overall pipeline of our PoseMaster. Given a single image and expected pose, our PoseMaster integrates them into a unified 3D native generation framework to achieve precise arbitrary-pose control for 3D characters.

can efficiently animate 3D characters to create our dataset using open-source MMD tools [4]. We collect approximately 10,000 characters from Playbox [5] and filter out anomalous data, such as non-humanoid and multi-object data. This process yields around 7K high-quality, artist-designed humanoid characters. The standardized MMD model data format ensures that all MMD character data includes skeletons with unified naming conventions. We take full advantage of this feature by collecting about 12 VMD animation files from Playbox [5]. For each character, we randomly select 10 VMD animations and extract 10 frames from each animation to export the character’s skeleton, image, and mesh. Consequently, we obtain approximately 60M data samples representing various poses. Note that, Errors such as rendering interruption caused incomplete data, so we only obtained 60M data.

4.1.2. Data processing

For the skeleton, we extracted the bone coordinates in the world coordinate system, with each bone defined by its starting and ending points. To ensure universality, we focus solely on standard body bones. For image rendering, we utilize a perspective camera to produce images at a resolution of 2048. Detailed information regarding the body bones and camera settings can be found in the supporting materials. For the character mesh, we follow the methodology outlined in Dora [12] to convert the original mesh into a watertight format, from which we then extract the Signed Distance Function (SDF) field, surface points, and sharp surface points. Given the complex geometric structures of 3D characters, we sample 49,512 surface points and 16,384 sharp points.

4.2. Arbitrary-pose 3D Character Generation

Similar to recent 3D native generation models [29, 67], our PoseMaster contains two primary component: 3D VAE and 3D diffusion model, as shown in Figure 2. The architecture of our 3D VAE is adapted from Dora [12]. To effectively represent complex 3D characters, we scale the input surface points and the latent vector length to 49,512 and 2,048, respectively. With these modifications, we fine-tune the original VAE from Dora. Building on this fine-tuned VAE, we develop a flow-based diffusion model to enable arbitrary-pose 3D character generation. We now describe how we effectively generate 3D characters with an arbitrary pose from a single image and a skeleton.

4.2.1. Condition Encoders

In our PoseMaster, there are two condition encoders: one for obtaining the image condition $c_i \in \mathbb{R}^{M \times C_i}$ and another for generating the pose condition $c_p \in \mathbb{R}^{N \times C_p}$. Here, the M and N denote the lengths of the conditions, while C_i and C_p indicate their respective dimensions. For the image input I_i , we employ the pretrained DINO-v2 [38] as our image encoder to derive the image condition, formulated as $c_i = DINO_{v2}(I_i)$.

For the pose condition, we propose using a 3D skeleton to provide sparse 3D structural information, in contrast to the 2D-image-based skeletons employed in previous character generation methods [20, 42]. A straightforward approach is to utilize the spatial coordinates of the skeleton joints. While joint positions are adequate for controlling simple poses like A-pose and T-pose, they are insufficient for conveying precise connection information in more complex poses, which can result in imprecise pose control.

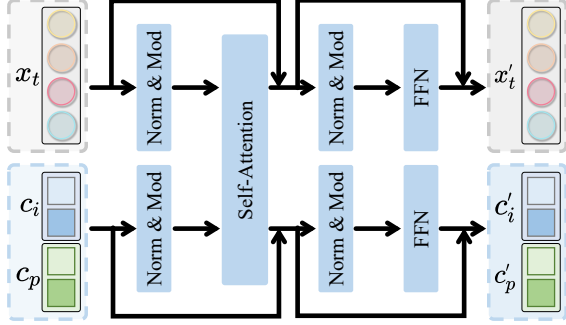


Figure 3. The structure of our DiT. We combine the image condition c_i and pose condition c_p as the joint condition and feed them with the latent x_t into a Transformer [15].

Therefore, we represent pose control using bones instead of joints. Each bone is represented by aggregating its starting and ending points. We define the starting points and ending points of each bone as $P_s \in \mathbb{R}^{N \times 3}$ and $P_e \in \mathbb{R}^{N \times 3}$. N is the number of bones. Our skeletal condition c_p and skeleton encoder ϕ_p can be formulated as follows:

$$c_p = \phi_p(P_s, P_e) = SA(\mathcal{T}(PE([P_s, P_e]))) \quad (4)$$

where $[\cdot]$ is the concatenation operation in dimension space. The expression $[P_s, P_e] \in \mathbb{R}^{N \times 6}$ represent a single bone in the skeleton. PE , \mathcal{T} , and SA refer to position embeddings, multi-layer perceptrons (MLPs), and self-attention layers, respectively. The self-attention layer is employed to learn the spatial relationships between bones.

4.2.2. Multi-Condition DiT

Recently, the Diffusion Transformer (DiT) [41] has been drawing extensive attention due to its efficiency and flexibility. Based on the DiT structure, recent native image-to-3D models [29, 57] have introduced several powerful methods for projecting image conditions. Following these methods and the recent advanced multi-modal Transformer proposed by Stable Diffusion 3 [15], we design our multi-condition DiT. As illustrated in Figure 3, we combine the image condition c_i and pose condition c_p to form a joint condition. After applying normalization and modulation operations, we concatenate the sequences of the joint condition with the latent codes x_t into a self-attention layer. For the modulating operation, we inherit PixArt [10] and CraftMan [29] to employ AdaLN-single [10] to reduce the number of parameters. Finally, we employ two separate MLPs to update the features of the latent codes x_t and the combined condition c . We can define our DiT v_θ as follows:

$$v_\theta(x_t, t, c_i, c_p) = \{SA([\mathcal{M}_1(x_t, t), \mathcal{M}_2([c_i, c_p], t)])\}^{24} \quad (5)$$

where \mathcal{M}_1 and \mathcal{M}_2 are modulate operation. For clarity, we omit certain elements like normalization and feed-forward layers in this equation.

Classifier-free Guidance. The Classifier-free Guidance (CFG) plays a vital role in the controllable and conditional generation. In the image-to-3D generation, the Classifier-free Guidance (CFG) of image condition c_i can be formulated by the following:

$$\tilde{x}_t = v_\theta(x_t, t, \emptyset) + \lambda \cdot (v_\theta(x_t, t, c_i) - v_\theta(x_t, t, \emptyset)) \quad (6)$$

where λ is the guidance scale. Following previous controllable generation methods [54, 69, 70], such as ControlNet [66], we can freeze the additional pose condition c_p , which can be represented as:

$$x_t = v_\theta(x_t, t, c_p, \emptyset) + \lambda \cdot (v_\theta(x_t, t, c_p, c_i) - v_\theta(x_t, t, c_p, \emptyset)) \quad (7)$$

In this setting, only the image condition c_i is required to be empty randomly in the training. However, we empirically observe that training the network with this strategy results in insufficient generalization, negatively impacting the quality of the generated outputs. To tackle this issue, we also randomly nullify the pose condition during the training phase. Furthermore, both the image condition and pose condition are nullified with independent probabilities. With this approach, we obtain four condition models, including: $v_\theta(x_t, t, \emptyset, \emptyset)$, $v_\theta(x_t, t, c_p, \emptyset)$, $v_\theta(x_t, t, \emptyset, c_i)$, $v_\theta(x_t, t, c_p, c_i)$. During inference, we can utilize the following simplified classifier-free guidance to predict noise x_t :

$$x_t = \lambda_1 * v_\theta(x_t, t, c_p, c_i) + \lambda_2 * v_\theta(x_t, t, c_p, \emptyset) + \lambda_3 * v_\theta(x_t, t, \emptyset, c_i) + \lambda_4 * v_\theta(x_t, t, \emptyset, \emptyset) \quad (8)$$

where $\lambda_1, \lambda_2, \lambda_3, \lambda_4$ are the guidance scale for each condition model.

5. Experiments

5.1. Implemental details

In this work, we train our model using the AnimePose dataset derived from Playbox [5]. For image condition extraction, we utilize DINO-v2-Large [38] at a resolution of 518 to extract image features with a length of $M = 1370$ and a dimension of $C_i = 1024$. For our pose condition, we set the length N and dimension C_p to 21 and 768, respectively. For our flow model, we first follow the setting of Dora [12, 25] to fine-tune our VAE. The diffusion model consists of 24 layers of DiT blocks, each with a dimension of 1024, totaling 517 million parameters. We directly train our diffusion model and skeleton encoder on our AnimePose dataset using a fixed learning rate of 1e-4 across 40 H20 GPUs.

5.2. Metrics and Baselines

To evaluate the generated posed 3D characters with assigned poses, we adopt geometric metrics similar to the

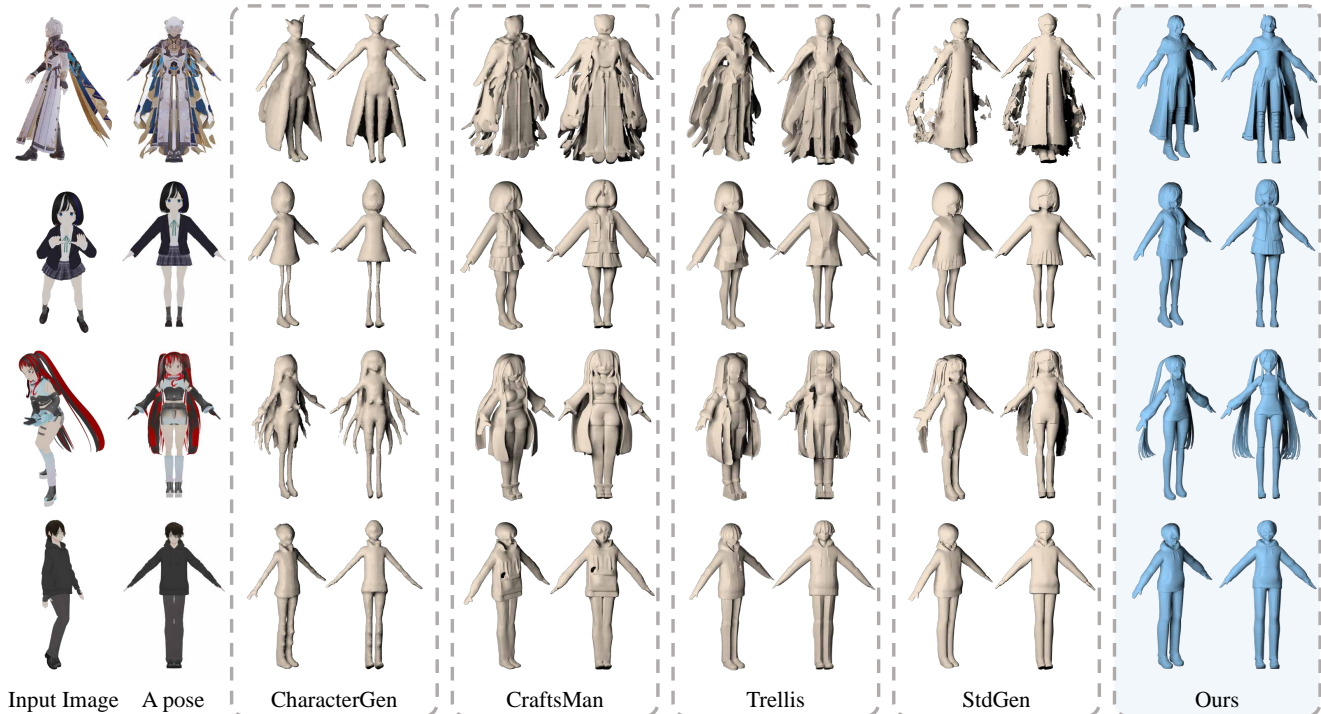


Figure 4. The qualitative comparison for A-pose character generation. Our method achieves higher geometry quality and accuracy compared with baselines.

benchmarks used in Dora [12], including Chamfer Distance (CD) and F1-score. Additionally, we introduce an extra metric, Fidelity Distance (FD), to assess the fidelity of the generated outputs. The FD measures the single-sided CD from the ground truth to the generated mesh. For A-pose generation, we conduct both qualitative and quantitative comparisons of our method against CraftsMan [29], Trellis [58], CharacterGen [42], and StdGen [16]. For CraftsMan and Trellis, we use A-pose images generated by StdGen as their inputs. All methods are evaluated on unseen data sourced from Playbox [5] and VRoid-Hub [6].

5.3. Results and Comparisons

5.3.1. A-pose 3D Character Generation

In this section, we present both quantitative and qualitative results demonstrating the effectiveness of our PoseMaster for A-pose character generation.

Quantitative comparison. As shown in Tab. 1, our PoseMaster achieves the best performance across all metrics. Notably, although our model was not trained on VRoid-Hub data[6], it still demonstrates superior performance in A-pose character generation compared to existing 2D transformation-based methods.

Qualitative Comparison. Figure 4 presents a visual comparison of our method against baseline approaches. To highlight the challenges faced, we include the intermediate

Data	Method	CD ↓	FD ↓	F1-score ↑
Playbox	CharacterGen [42]	0.0438	0.046	0.2100
	CraftsMan [29]	0.0481	0.0421	0.2112
	Trellis [58]	0.0476	0.0445	0.2072
	StdGen [16]	0.0437	0.0439	0.2304
	PoseMaster	0.0331	0.0385	0.3040
VRoid	CharacterGen [42]	0.0372	0.0378	0.2419
	CraftsMan [29]	0.0319	0.0310	0.2484
	Trellis [58]	0.0259	0.0264	0.3135
	StdGen [16]	0.0249	0.0269	0.3203
	PoseMaster	0.0197	0.0228	0.4735

Table 1. Quantitative comparison for A-pose 3D character generation on the testing dataset sampled from Playbox [5] and VRoid [6].

A-pose image generated by StdGen (second column). This visualization reveals that pose transformation in 2D space is highly vulnerable to issues such as self-occlusion, viewpoint changes, and pose variations, resulting in various artifacts and distortions. As a consequence, subsequent image-to-3D models, including advanced native generation models like CraftMan [29] and Trellis [58], struggle to accurately reconstruct A-pose 3D characters. For example, in the second and last samples, StdGen’s A-pose image displays leg distortion, leading to final 3D outputs that deviate from the

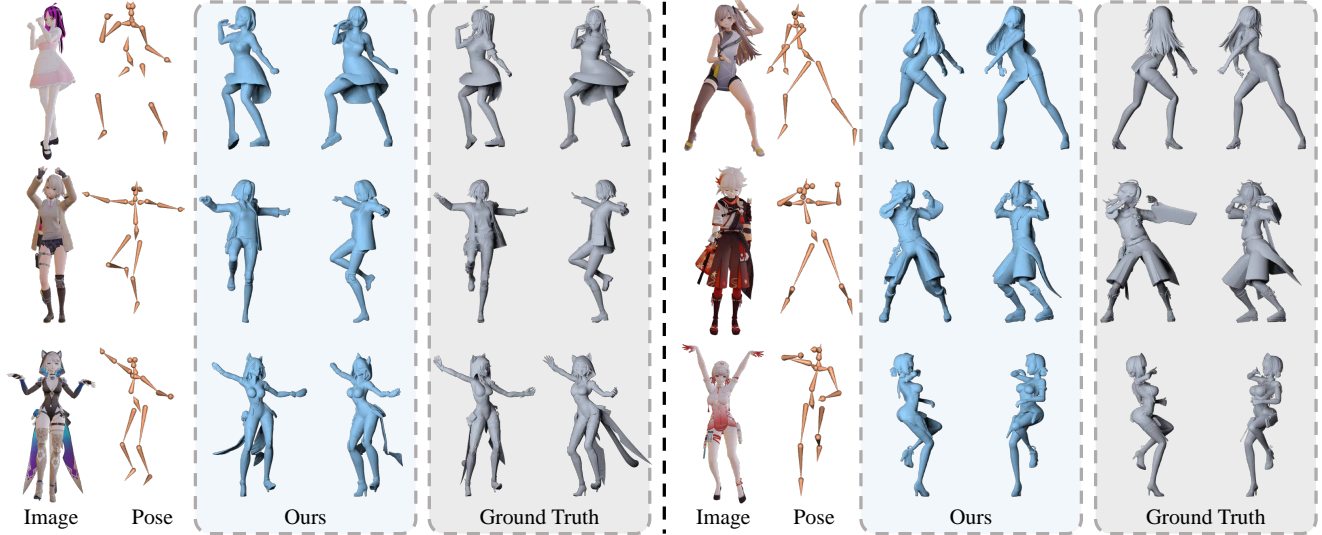


Figure 5. The visualization for arbitrary-pose 3D character generation for our PoseMaster.

Method	Time
CharacterGen [42]	~ 60 (s)
StdGen [16]	~ 180 (s)
Our PoseMaster	~ 3 (s)

Table 2. Time comparison for generating an A-pose 3D character. Our method only requires 3 seconds.

standard A-pose. In contrast, our PoseMaster framework integrates pose transformation and 3D generation, effectively preserving the original image information. By utilizing a 3D skeleton as guidance, our model generates more precise A-poses, as illustrated by the samples at the bottom of Figure 4. Both quantitative and qualitative evaluations consistently demonstrate PoseMaster’s ability to produce high-quality 3D characters.

Generation Speed. We further compare the generation speed of our method with other 3D character generation approaches in Table 2. Our method demonstrates significantly faster generation speeds, being 20 times faster than CharacterGen [42] and 60 times faster than StdGen [16]. This speed advantage is primarily due to PoseMaster’s integrated single-stage generative framework, which eliminates the dependence on multi-stage generation pipelines used in previous methods [16, 42].

Textured mesh comparison. We also performed a qualitative comparison of our method with CharacterGen [42] and StdGen [16] on A-pose meshes with applied textures. As shown in Fig. 12 and 13, high-quality geometry is essential for achieving superior texture quality. As an end-to-end model, PoseMaster effectively retains input information

from the original image, allowing for the recovery of geometric details, such as hair and clothing embellishments. These intricate geometries are vital for subsequent texture mapping, which accounts for our method’s better texture results compared to CharacterGen and StdGen.

5.3.2. Arbitrary-pose 3D Character Generation

Beyond A-pose generation, our method greatly improves controllability for producing characters in arbitrary poses. In contrast, traditional methods depend on complex and specialized post-processing (i.e., rigging and skinning) to achieve varied poses, which is a challenging task for the common customer. With PoseMaster, users can simply specify a desired pose to directly generate the corresponding 3D character. Although automatic rigging tools like Mixamo [2] are available, they often encounter difficulties with intricate areas such as hair and skirts, particularly in terms of accurate skinning weights, as illustrated in our appendix.

Figure 5 visualizes input images, skeletons, and our generated results alongside ground truth, effectively showcasing the pose control capabilities of PoseMaster. Notably, even in the absence of explicit skeletal guidance for elements like hair and clothing, PoseMaster adaptively transforms these components based on the body pose. This demonstrates that PoseMaster has learned essential physical priors from the data, allowing it to avoid generating unrealistic or interpenetrating structures. Overall, PoseMaster excels not only in generating high-quality rest-pose 3D characters but also in producing characters in more complex poses, significantly enhancing customized pose generation.

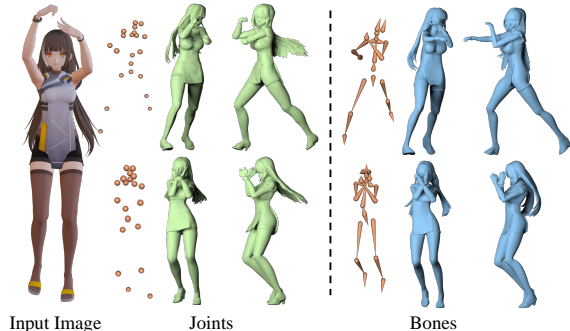


Figure 6. The qualitative comparison between different pose representations in terms of joints and bones of skeleton.

5.4. Ablation Study

5.4.1. Effect of pose representation

We investigated the effect of pose representation on arbitrary-pose control, specifically comparing the accuracy of joint-based versus bone-based signals. Our experiments revealed that while joints, as pose control signals, accurately control simple poses, they struggle with complex configurations, such as crossed arms (Figure 6). This limitation arises because joints merely provide point positions, preventing the network from inferring crucial connectivity information necessary for accurate complex pose reconstruction. In contrast, using bones as a pose representation effectively addresses this limitation. Each bone, defined by its start and end points and connected via joints, offers a more robust and complete skeletal representation. Figure 6 visually confirms these advantages.

5.4.2. Effect of CFG

In this study, we aim to explore the effects of the different CFG strategies for the multi-condition generation model. For clarity, we define the diffusion model using the CFG strategy corresponding to Equation 7 as Eq. 7, and the model using the CFG strategy corresponding to Equation 8 as Eq. 8. We set the guidance weight λ for Eq. 7 to 7.5. We employ ‘‘A’’ and ‘‘B’’ to differentiate the models of using Eq. 8 with different guidance weights. For Eq. 8-A, the parameters λ_1 , λ_2 , λ_3 , and λ_4 are set to 7.5, -6.5, 0, 0, respectively. In contrast, for Eq. 8-B, these parameters are set to 14.5, -7, -3, -3, respectively. The main difference between Eq. 7 and Eq. 8-A is the introduction of the unconditional model concerning pose condition c_p in the training stage. The comparison between Eq. 7 and Eq. 8-A, shown in Figure 7, indicates that the unconditional model helps smooth the final generated results. Furthermore, the comparison between Eq. 8-A and Eq. 8-B reveals that the model’s generalizability is influenced by the unconditional models for both image and pose conditions.

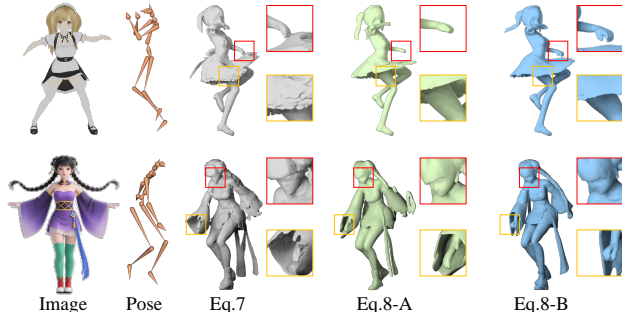


Figure 7. The qualitative comparison between the different CFG strategies in the training.

6. Conclusion

In this paper, we propose PoseMaster, a unified framework for achieving arbitrary-pose 3D character generation from arbitrary-pose image inputs. Unlike previous methods that use separate models for pose standardization and 3D reconstruction, we integrate pose transformation and character generation into a single flow-based generative framework based on recent native 3D generation techniques. To enhance the accuracy of pose control, we utilize a 3D skeleton as the pose representation, which provides precise pose information and offers sparse 3D structural data. Additionally, to address the specificity of multi-conditional control, we randomly omit the pose condition and the image condition during training to improve the effectiveness and generalizability of pose control. Finally, to train our model and enable it to learn the implicit relationships between the skeleton and skinning weights, we create a dataset derived from realistic character animation data. Several experiments demonstrate that PoseMaster outperforms existing A-pose 3D character generation methods in terms of quality and speed while achieving effective and efficient arbitrary-pose 3D character generation within a unified framework.

References

- [1] Blender, 2025. <https://www.blender.org/>. 13
- [2] Mixamo, 2025. <https://www.mixamo.com>. 7, 12
- [3] Mikumikudance, 2025. <https://zh.wikipedia.org/wiki/MikuMikuDance>. 3
- [4] Mmd tools, 2025. <https://extensions.blender.org/add-ons/mmd-tools/>. 4
- [5] Playbox, 2025. <https://www.aplaybox.com>. 4, 5, 6, 12, 13, 14
- [6] Vroid-hub, 2025. <https://hub.vroid.com/>. 6, 12, 14
- [7] Thiemo Aaldieck, Hongyi Xu, and Cristian Sminchisescu. imghum: Implicit generative models of 3d human shape and articulated pose. In *Proceedings of the IEEE/CVF International Conference on Computer Vision*, pages 5461–5470, 2021. 3

- [8] Yukang Cao, Yan-Pei Cao, Kai Han, Ying Shan, and Kwan-Yee K Wong. Dreamavatar: Text-and-shape guided 3d human avatar generation via diffusion models. *arXiv preprint arXiv:2304.00916*, 2023. 2, 3
- [9] Zhe Cao, Gines Hidalgo, Tomas Simon, Shih-En Wei, and Yaser Sheikh. Openpose: Realtime multi-person 2d pose estimation using part affinity fields. *IEEE transactions on pattern analysis and machine intelligence*, 43(1):172–186, 2019. 12
- [10] Junsong Chen, Jincheng Yu, Chongjian Ge, Lewei Yao, Enze Xie, Yue Wu, Zhongdao Wang, James Kwok, Ping Luo, Huchuan Lu, and Zhenguo Li. Pixart- α : Fast training of diffusion transformer for photorealistic text-to-image synthesis, 2023. 5
- [11] Rui Chen, Yongwei Chen, Ningxin Jiao, and Kui Jia. Fantasia3d: Disentangling geometry and appearance for high-quality text-to-3d content creation. In *Proceedings of the IEEE/CVF International Conference on Computer Vision (ICCV)*, 2023. 2
- [12] Rui Chen, Jianfeng Zhang, Yixun Liang, Guan Luo, Weiyu Li, Jiarui Liu, Xiu Li, Xiaoxiao Long, Jiashi Feng, and Ping Tan. Dora: Sampling and benchmarking for 3d shape variational auto-encoders. *arXiv preprint arXiv:2412.17808*, 2024. 4, 5, 6
- [13] Zhiqin Chen and Hao Zhang. Learning implicit fields for generative shape modeling. In *Conference on Computer Vision and Pattern Recognition (CVPR)*, pages 5939–5948, 2019. 3
- [14] Matt Deitke, Dustin Schwenk, Jordi Salvador, Luca Weihs, Oscar Michel, Eli VanderBilt, Ludwig Schmidt, Kiana Ehsani, Aniruddha Kembhavi, and Ali Farhadi. Objaverse: A universe of annotated 3d objects. In *Proceedings of the IEEE/CVF Conference on Computer Vision and Pattern Recognition*, pages 13142–13153, 2023. 2
- [15] Patrick Esser, Sumith Kulal, Andreas Blattmann, Rahim Entezari, Jonas Müller, Harry Saini, Yam Levi, Dominik Lorenz, Axel Sauer, Frederic Boesel, et al. Scaling rectified flow transformers for high-resolution image synthesis. In *Forty-first international conference on machine learning*, 2024. 5
- [16] Yuze He, Yanning Zhou, Wang Zhao, Zhongkai Wu, Kaiwen Xiao, Wei Yang, Yong-Jin Liu, and Xiao Han. Stdgen: Semantic-decomposed 3d character generation from single images. *arXiv preprint arXiv:2411.05738*, 2024. 2, 3, 6, 7, 13
- [17] Fangzhou Hong, Zhaoxi Chen, Yushi Lan, Liang Pan, and Ziwei Liu. Eva3d: Compositional 3d human generation from 2d image collections. *arXiv preprint arXiv:2210.04888*, 2022. 3
- [18] Fangzhou Hong, Mingyuan Zhang, Liang Pan, Zhongang Cai, Lei Yang, and Ziwei Liu. Avatarclip: Zero-shot text-driven generation and animation of 3d avatars. 2022. 3
- [19] Yicong Hong, Kai Zhang, Jiuxiang Gu, Sai Bi, Yang Zhou, Difan Liu, Feng Liu, Kalyan Sunkavalli, Trung Bui, and Hao Tan. Lrm: Large reconstruction model for single image to 3d. *arXiv preprint arXiv:2311.04400*, 2023. 2, 3
- [20] Yukun Huang, Jianan Wang, Ailing Zeng, He Cao, Xianbiao Qi, Yukai Shi, Zheng-Jun Zha, and Lei Zhang. Dreamwaltz: Make a scene with complex 3d animatable avatars. *Advances in Neural Information Processing Systems*, 36:4566–4584, 2023. 3, 4
- [21] Yangyi Huang, Hongwei Yi, Yuliang Xiu, Tingting Liao, Ji-axiang Tang, Deng Cai, and Justus Thies. Tech: Text-guided reconstruction of lifelike clothed humans. In *2024 International Conference on 3D Vision (3DV)*, pages 1531–1542. IEEE, 2024. 3
- [22] Ruixiang Jiang, Can Wang, Jingbo Zhang, Menglei Chai, Mingming He, Dongdong Chen, and Jing Liao. Avatarcraft: Transforming text into neural human avatars with parameterized shape and pose control. In *Proceedings of the IEEE/CVF International Conference on Computer Vision*, pages 14371–14382, 2023. 2, 3
- [23] Bernhard Kerbl, Georgios Kopanas, Thomas Leimkühler, and George Drettakis. 3d gaussian splatting for real-time radiance field rendering. *ToG*, 2023. 2
- [24] Nikos Kolotouros, Thiemo Alldieck, Andrei Zanfir, Eduard Bazavan, Mihai Fieraru, and Cristian Sminchisescu. Dreamhuman: Animatable 3d avatars from text. *Advances in Neural Information Processing Systems*, 36:10516–10529, 2023. 3
- [25] Zeqiang Lai, Yunfei Zhao, Zibo Zhao, Haolin Liu, Fuyun Wang, Huiwen Shi, Xianghui Yang, Qinxiang Lin, Jinwei Huang, Yuhong Liu, Jie Jiang, Chunchao Guo, and Xiangyu Yue. Unleashing vecset diffusion model for fast shape generation, 2025. 5
- [26] Chun-Liang Li, Manzil Zaheer, Yang Zhang, Barnabas Poczozos, and Ruslan Salakhutdinov. Point cloud gan. *arXiv preprint arXiv:1810.05795*, 2018. 3
- [27] Sixu Li, Chaojian Li, Wenbo Zhu, Boyang Yu, Yang Zhao, Cheng Wan, Haoran You, Huihong Shi, and Yingyan Lin. Instant-3d: Instant neural radiance field training towards on-device ar/vr 3d reconstruction. In *Proceedings of the 50th Annual International Symposium on Computer Architecture*, pages 1–13, 2023. 2
- [28] Weiyu Li, Rui Chen, Xuelin Chen, and Ping Tan. Sweetdreamer: Aligning geometric priors in 2d diffusion for consistent text-to-3d. *International Conference on Learning Representations (ICLR)*, 2024. 2
- [29] Weiyu Li, Jiarui Liu, Rui Chen, Yixun Liang, Xuelin Chen, Ping Tan, and Xiaoxiao Long. Craftsman: High-fidelity mesh generation with 3d native generation and interactive geometry refiner. *arXiv preprint arXiv:2405.14979*, 2024. 2, 3, 4, 5, 6
- [30] Yixun Liang, Xin Yang, Jiantao Lin, Haodong Li, Xiaogang Xu, and Yingcong Chen. Luciddreamer: Towards high-fidelity text-to-3d generation via interval score matching. *arXiv preprint arXiv:2311.11284*, 2023. 2
- [31] Tingting Liao, Hongwei Yi, Yuliang Xiu, Ji-axiang Tang, Yangyi Huang, Justus Thies, and Michael J Black. Tada! text to animatable digital avatars. In *2024 International Conference on 3D Vision (3DV)*, pages 1508–1519. IEEE, 2024. 3
- [32] Chen-Hsuan Lin, Jun Gao, Luming Tang, Towaki Takikawa, Xiaohui Zeng, Xun Huang, Karsten Kreis, Sanja Fidler, Ming-Yu Liu, and Tsung-Yi Lin. Magic3d: High-resolution text-to-3d content creation. In *CVPR*, 2023. 2

- [33] Xingchao Liu, Chengyue Gong, and Qiang Liu. Flow straight and fast: Learning to generate and transfer data with rectified flow. *arXiv preprint arXiv:2209.03003*, 2022. 2, 3
- [34] Zhen Liu, Yao Feng, Michael J. Black, Derek Nowrouzezahrai, Liam Paull, and Weiyang Liu. Meshdiffusion: Score-based generative 3d mesh modeling. In *International Conference on Learning Representations*, 2023. 3
- [35] Matthew Loper, Naureen Mahmood, Javier Romero, Gerard Pons-Moll, and Michael J Black. Smpl: A skinned multi-person linear model. In *Seminal Graphics Papers: Pushing the Boundaries, Volume 2*, pages 851–866. 2023. 2, 3
- [36] Ben Mildenhall, Pratul P. Srinivasan, Matthew Tancik, Jonathan T. Barron, Ravi Ramamoorthi, and Ren Ng. Nerf: Representing scenes as neural radiance fields for view synthesis. In *European Conference on Computer Vision (ECCV)*, 2020. 2
- [37] Charlie Nash, Yaroslav Ganin, SM Ali Eslami, and Peter Battaglia. Polygen: An autoregressive generative model of 3d meshes. In *International conference on machine learning*, pages 7220–7229. PMLR, 2020. 3
- [38] Maxime Oquab, Timothée Darcet, Theo Moutakanni, Huy V. Vo, Marc Szafraniec, Vasil Khalidov, Pierre Fernandez, Daniel Haziza, Francisco Massa, Alaaeldin El-Nouby, Russell Howes, Po-Yao Huang, Hu Xu, Vasu Sharma, Shang-Wen Li, Wojciech Galuba, Mike Rabbat, Mido Assran, Nicolas Ballas, Gabriel Synnaeve, Ishan Misra, Herve Jegou, Julien Mairal, Patrick Labatut, Armand Joulin, and Piotr Bojanowski. Dinov2: Learning robust visual features without supervision, 2023. 4, 5
- [39] Jeong Joon Park, Peter Florence, Julian Straub, Richard Newcombe, and Steven Lovegrove. Deepsdf: Learning continuous signed distance functions for shape representation. In *Conference on Computer Vision and Pattern Recognition (CVPR)*, pages 165–174, 2019. 3
- [40] Georgios Pavlakos, Vasileios Choutas, Nima Ghorbani, Timo Bolkart, Ahmed AA Osman, Dimitrios Tzionas, and Michael J Black. Expressive body capture: 3d hands, face, and body from a single image. In *Proceedings of the IEEE/CVF conference on computer vision and pattern recognition*, pages 10975–10985, 2019. 3
- [41] William Peebles and Saining Xie. Scalable diffusion models with transformers. In *Proceedings of the IEEE/CVF international conference on computer vision*, pages 4195–4205, 2023. 5
- [42] Hao-Yang Peng, Jia-Peng Zhang, Meng-Hao Guo, Yan-Pei Cao, and Shi-Min Hu. Charactergen: Efficient 3d character generation from single images with multi-view pose canonicalization. *ACM Transactions on Graphics (TOG)*, 43(4): 1–13, 2024. 2, 3, 4, 6, 7, 13
- [43] Ben Poole, Ajay Jain, Jonathan T Barron, and Ben Mildenhall. Dreamfusion: Text-to-3d using 2d diffusion. *arXiv preprint arXiv:2209.14988*, 2022. 2
- [44] Xuanchi Ren, Jiahui Huang, Xiaohui Zeng, Ken Museth, Sanja Fidler, and Francis Williams. Xcube: Large-scale 3d generative modeling using sparse voxel hierarchies. In *Proceedings of the IEEE/CVF Conference on Computer Vision and Pattern Recognition*, 2024. 3
- [45] Nataniel Ruiz, Yuanzhen Li, Varun Jampani, Yael Pritch, Michael Rubinstein, and Kfir Aberman. Dreambooth: Fine tuning text-to-image diffusion models for subject-driven generation. In *Proceedings of the IEEE/CVF conference on computer vision and pattern recognition*, pages 22500–22510, 2023. 3
- [46] Tianchang Shen, Jun Gao, Kangxue Yin, Ming-Yu Liu, and Sanja Fidler. Deep marching tetrahedra: a hybrid representation for high-resolution 3d shape synthesis. *Advances in Neural Information Processing Systems*, 34:6087–6101, 2021. 2
- [47] Yichun Shi, Peng Wang, Jianglong Ye, Long Mai, Kejie Li, and Xiao Yang. Mvdream: Multi-view diffusion for 3d generation. *arXiv:2308.16512*, 2023. 2
- [48] Yawar Siddiqui, Antonio Alliegro, Alexey Artemov, Tatiana Tommasi, Daniele Sirigatti, Vladislav Rosov, Angela Dai, and Matthias Nießner. Meshgpt: Generating triangle meshes with decoder-only transformers. In *Proceedings of the IEEE/CVF conference on computer vision and pattern recognition*, pages 19615–19625, 2024. 3
- [49] Jiayang Tang, Jiawei Ren, Hang Zhou, Ziwei Liu, and Gang Zeng. Dreamgaussian: Generative gaussian splatting for efficient 3d content creation. *arxiv*, 2023. 2
- [50] Jiayang Tang, Zhaoxi Chen, Xiaokang Chen, Tengfei Wang, Gang Zeng, and Ziwei Liu. Lgm: Large multi-view gaussian model for high-resolution 3d content creation. *arXiv preprint arXiv:2402.05054*, 2024. 2
- [51] Tencent. Hunyuan 3d, 2025. <https://3d.hunyuan.tencent.com>. 13
- [52] VAST. Tripo 3d, 2025. <https://www.tripo3d.ai/app/home>. 13
- [53] Ashish Vaswani, Noam Shazeer, Niki Parmar, Jakob Uszkoreit, Llion Jones, Aidan N Gomez, Łukasz Kaiser, and Illia Polosukhin. Attention is all you need. *Advances in neural information processing systems*, 30, 2017. 2
- [54] Haoxuan Wang, Jinlong Peng, Qingdong He, Hao Yang, Ying Jin, Jiafu Wu, Xiaobin Hu, Yanjie Pan, Zhenye Gan, Mingmin Chi, et al. Unicombine: Unified multi-conditional combination with diffusion transformer. *arXiv preprint arXiv:2503.09277*, 2025. 5
- [55] Zhengyi Wang, Cheng Lu, Yikai Wang, Fan Bao, Chongxuan Li, Hang Su, and Jun Zhu. Prolificdreamer: High-fidelity and diverse text-to-3d generation with variational score distillation. *arXiv preprint arXiv:2305.16213*, 2023. 2
- [56] Zhengyi Wang, Yikai Wang, Yifei Chen, Chendong Xi-ang, Shuo Chen, Dajiang Yu, Chongxuan Li, Hang Su, and Jun Zhu. Crm: Single image to 3d textured mesh with convolutional reconstruction model. *arXiv preprint arXiv:2403.05034*, 2024. 2
- [57] Shuang Wu, Youtian Lin, Feihu Zhang, Yifei Zeng, Jingxi Xu, Philip Torr, Xun Cao, and Yao Yao. Direct3d: Scalable image-to-3d generation via 3d latent diffusion transformer. *arXiv preprint arXiv:2405.14832*, 2024. 5
- [58] Jianfeng Xiang, Zelong Lv, Sicheng Xu, Yu Deng, Ruicheng Wang, Bowen Zhang, Dong Chen, Xin Tong, and Jiaolong Yang. Structured 3d latents for scalable and versatile 3d generation. *arXiv preprint arXiv:2412.01506*, 2024. 6
- [59] Jiale Xu, Weihao Cheng, Yiming Gao, Xintao Wang, Shenghua Gao, and Ying Shan. Instantmesh: Efficient 3d

mesh generation from a single image with sparse-view large reconstruction models. *arXiv preprint arXiv:2404.07191*, 2024. 2

- [60] Yinghao Xu, Hao Tan, Fujun Luan, Sai Bi, Peng Wang, Jiahao Li, Zifan Shi, Kalyan Sunkavalli, Gordon Wetzstein, Zexiang Xu, et al. Dmv3d: Denoising multi-view diffusion using 3d large reconstruction model. *arXiv preprint arXiv:2311.09217*, 2023. 2
- [61] Guandao Yang, Xun Huang, Zekun Hao, Ming-Yu Liu, Serge Belongie, and Bharath Hariharan. Pointflow: 3d point cloud generation with continuous normalizing flows. *arXiv*, 2019. 3
- [62] Taoran Yi, Jiemin Fang, Junjie Wang, Guanjun Wu, Lingxi Xie, Xiaopeng Zhang, Wenyu Liu, Qi Tian, and Xinggang Wang. Gaussiandreamer: Fast generation from text to 3d gaussians by bridging 2d and 3d diffusion models. In *Proceedings of the IEEE/CVF Conference on Computer Vision and Pattern Recognition*, pages 6796–6807, 2024. 2
- [63] Biao Zhang, Jiapeng Tang, Matthias Niessner, and Peter Wonka. 3dshape2vecset: A 3d shape representation for neural fields and generative diffusion models. *ACM Transactions on Graphics (TOG)*, 42(4):1–16, 2023. 3
- [64] Huichao Zhang, Bowen Chen, Hao Yang, Liao Qu, Xu Wang, Li Chen, Chao Long, Feida Zhu, Kang Du, and Min Zheng. Avatarverse: High-quality & stable 3d avatar creation from text and pose. 2023. 3
- [65] Kai Zhang, Sai Bi, Hao Tan, Yuanbo Xiangli, Nanxuan Zhao, Kalyan Sunkavalli, and Zexiang Xu. Gs-lrm: Large reconstruction model for 3d gaussian splatting. *arXiv preprint arXiv:2404.19702*, 2024. 2
- [66] Lvmin Zhang, Anyi Rao, and Maneesh Agrawala. Adding conditional control to text-to-image diffusion models. In *Proceedings of the IEEE/CVF international conference on computer vision*, pages 3836–3847, 2023. 3, 5
- [67] Longwen Zhang, Ziyu Wang, Qixuan Zhang, Qiwei Qiu, Anqi Pang, Haoran Jiang, Wei Yang, Lan Xu, and Jingyi Yu. Clay: A controllable large-scale generative model for creating high-quality 3d assets. *ACM Transactions on Graphics (TOG)*, 43(4):1–20, 2024. 2, 3, 4
- [68] Xuanmeng Zhang, Jianfeng Zhang, Chenxu Zhang, Jun Hao Liew, Huichao Zhang, Yi Yang, and Jiashi Feng. Avatarstudio: High-fidelity and animatable 3d avatar creation from text. *International Journal of Computer Vision*, pages 1–19, 2025. 3
- [69] Yuxuan Zhang, Yirui Yuan, Yiren Song, Haofan Wang, and Jiaming Liu. Easycontrol: Adding efficient and flexible control for diffusion transformer. *arXiv preprint arXiv:2503.07027*, 2025. 5
- [70] Shihao Zhao, Dongdong Chen, Yen-Chun Chen, Jianmin Bao, Shaozhe Hao, Lu Yuan, and Kwan-Yee K Wong. Uni-controlnet: All-in-one control to text-to-image diffusion models. *Advances in Neural Information Processing Systems*, 36:11127–11150, 2023. 5
- [71] Linqi Zhou, Yilun Du, and Jiajun Wu. 3d shape generation and completion through point-voxel diffusion. In *Proceedings of the IEEE/CVF international conference on computer vision*, pages 5826–5835, 2021. 3

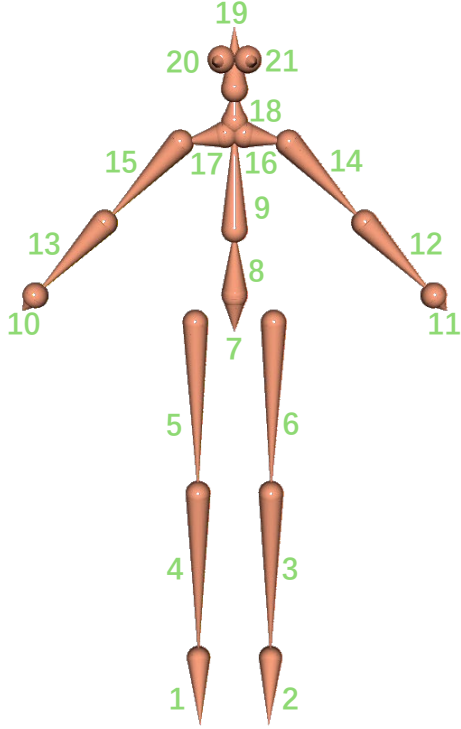


Figure 8. The 21 standard body bones used in pose condition.

7. Appendix

7.1. Texture generation

In this paper, we primarily focus on the geometric generation of controllable 3D characters and do not incorporate any specific design for texture generation. Our texture results are derived from UniText [1].

7.2. Data Details

As illustrated in Figure 8, we visualize the 21 standard body bones used in our pose condition, which primarily consist of the arms, legs, spine, and head, similar to the structure used in OpenPose [9]. For the rendering setup in Blender, we randomize the elevation angle between 0 and 10 degrees. We configure the camera’s field of view (FoV) to 50° and calculate the optimal distance between the camera and the animated character to ensure centered rendering frames.

7.3. AnimePose Benchmark

Our AnimePose benchmark comprises two evaluation datasets for A-pose 3D character generation tasks. The testing dataset is constructed using characters from Playbox [5] and VRoid-Hub [6]. In total, 37 characters are sourced from Playbox, while 24 characters come from VRoid-Hub [6]. Each character includes 1 to 2 images in arbitrary poses. For the arbitrary-pose generation task, we utilize unseen characters and skeleton motion sequences to assess the controlla-

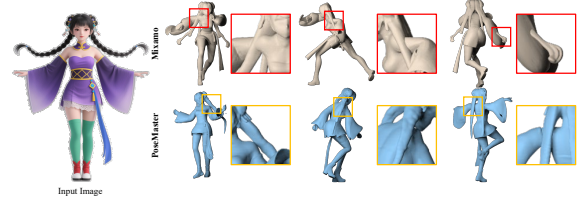


Figure 9. The comparison between our PoseMaster and auto-rigging tools [2] for pose transformation.

bility and generalizability of our method.

7.4. More Experiments

As shown in Figure 14, we present additional results with textures for arbitrary-pose 3D character generation. It is important to note that mismatches in pose between our input images and the posed mesh can result in inaccuracies in the texture mapping outcomes. In future work, we plan to explore optimizing the texture mapping approach to better accommodate this specific situation.

Comparison with auto-rigging tools. We further compare our arbitrary-pose generation with auto-rigging methods that can also achieve pose transformation. Specifically, we visualize the motion results for pose transformation using auto-rigging tools. We generate a T-pose 3D character and then use Mixamo [2] to obtain the rigging result, followed by applying Mixamo’s motion “Capoeire” to achieve the final motion results. Due to inconsistencies in the skeletal systems between Mixamo and Playbox, we are unable to compare the variations under the same pose. However, as shown in Figure 9, we observe that even after rigging with Mixamo, areas such as hair do not adjust their positions according to the pose transformation. In contrast, our PoseMaster modifies other parts, such as hair, based on the body pose. Furthermore, this adjustment does not require any additional operations, such as skinning. This comparison highlights the significant advantages of PoseMaster in generating arbitrary poses, particularly in terms of convenience, efficiency, and quality.

Application on animation. One of the goals for controllable generation is animation. Currently, the production of 3D animatable characters typically involves a rigging and skinning process, which usually relies on characters in rest poses, such as the A-pose and T-pose. In addition to manual rigging and skinning performed by artists, there are various automated rigging and skinning tools available. Different auto-rigging systems have specific requirements for the standard pose. Although both A-pose and T-pose can be considered rest poses, their differences can impact performance. For example, Mixamo [2] recommends using T-pose characters for automatic rigging. Furthermore, the angle between the upper arms and torso in the A-pose can vary, allowing for angles of 35°, 45°, 50°, and 55°. Dif-

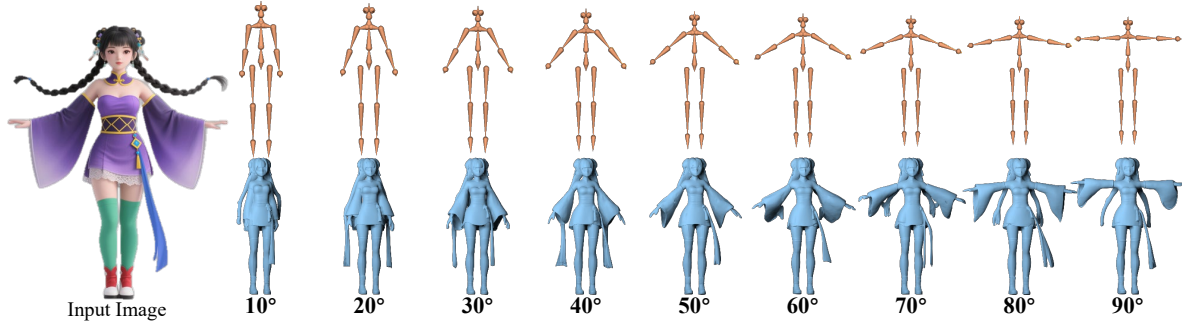


Figure 10. The visualized results demonstrate precise pose control. Given body bones with varying arm angles, our PoseMaster can generate 3D characters that accurately reflect the specified arm angles.

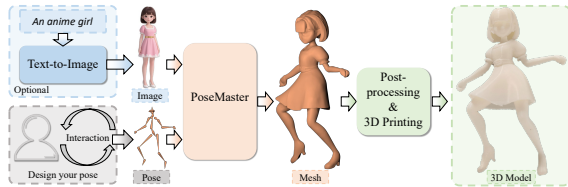


Figure 11. The system of 3D printing based on our PoseMaster. With our PoseMaster, we can style the pose of a single image for anime figure printing.

ferent characters in Playbox [5] exhibit varying arm angles in the A-pose, highlighting the need for precise control over different poses. However, previous methods, such as CharacterGen [42] and StdGen [16], could only generate the A-pose with a fixed 45° angle and struggled to produce A-poses with different angles. In contrast, PoseMaster can easily generate standard poses with varying angles. As shown in Figure 10, we applied different angles of the standard pose to a single image input from a T2I model and obtained the corresponding 3D results. The visualized outcomes demonstrate impressive consistency in arm angle between the generated mesh and the skeleton. This capability reveals that PoseMaster can achieve accurate pose control, significantly enhancing its value for downstream applications.

Application on 3D printing. Benefiting from the function of arbitrary-pose control, we can design a 3D printing system for anime characters. As shown in Figure 11, we first obtain a virtual 2D anime character from text-to-image models. Then, we design the desired pose using Blender [1] or pose editing tools (e.g., OpenPose Editor). Next, we export the bones of the skeleton and use PoseMaster to generate a 3D character based on the input image and pose. Finally, after a post-processing stage, a 3D anime figure in the expected pose is printed.

7.5. Limitation and Discussion

In this paper, we do not incorporate gesture control, resulting in challenges for our method in generating high-quality hand poses under complex pose guidance. However, for simple poses like the A-pose, our method is able to form accurate hand poses. To address this issue, we plan to incorporate hand bones into our pose condition in future work. Additionally, due to limitations in computational and storage resources, we have constructed only 7K characters with a model size of 517 MB. This limitation prevents our model from achieving the high-quality geometry observed in recent commercial and closed-source models, such as Hunyuan-3D [51] and Tripo3D [52]. Therefore, in future work, we aim to scale up our data and model size.



Figure 12. The qualitative comparison for textured mesh on the data from Playbox [5] and VRoid-Hub [6]



Figure 13. The qualitative comparison for textured mesh on the data from CharacterGen’s testing dataset



Figure 14. The textured results for arbitrary-pose 3D character generation for our PoseMaster.